Machine Learning Based Wavelength Modulation Spectroscopy for Rapid Gas Sensing

Machine Leaning Based Wavelength Modulation Spectroscopy for Rapid Gas Sensing

Wanlu Zhang, Rui Zhang, Yalei Fu, Godwin Enemali, Jingjing Si, Chang Liu*
School of Engineering, The University of Edinburgh, Edinburgh, United Kingdom
Email: C.Liu@ed.ac.uk

***Abstract*—As a non-intrusive, fast-response and highly sensitive and diagnostic tool, Wavelength Modulation Spectroscopy (WMS) has been extensively applied in accurate retrieval of gas properties, e.g. species concentration and temperature. Using the calibration-free WMS (CF-WMS) strategy, the first harmonic normalised second harmonic signal, e.g. 2*f*/1*f*, of the modulated laser transmission is extracted, and then fitted to calculate the path-integrated absorbance. However, the fitting process mainly suffers from (a) noise in the fitting results introduced by the shift of the centre wavelength of the laser, and (b) a relatively high computational cost due to the least square optimisation. To improve the measurement precision and efficiency, this paper proposes a machine learning regression algorithm to calculate the gas properties. The proposed method employs artificial neural networks (ANN) to compute the path-integrated absorbance rapidly with a high signal-to-noise ratio, which was experimentally validated by calculating the absorption of water vapour at the wavelength of 1391.2 nm. In comparison with the traditional fitting method, the proposed machine learning based WMS is two times more noise-resistant with high capability to compute 100 sets of 2*f*/1*f* signals in approximately 0.4 s, denoting its potential applicability in real-time and rapid trace gas sensing.**

***Keywords*—Artificial Neural Networks (ANN), Gas Sensing, Machine Learning, Wavelength Modulation Spectroscopy (WMS)**

I. Introduction

Gas sensing technique has been highly applied in a variety of industrial applications [1-3]. In Tunable Diode Laser Absorption Spectroscopy (TDLAS) systems, tunable diode lasers are applied to generate lasers passing through the target gas. The transmission signal detected by photodiode detectors can be processed to determine the gas compositions and properties [4-6]. As one of the representative TDLAS techniques, WMS is implemented by imposing high-frequency modulation on the low-frequency wavelength scan [2, 3]. Generally, strong noise rejection is achieved by the demodulation of WMS signal [7-9]. To facilitate the industrial implementation of WMS, the calibration-free WMS (CF-WMS) was proposed mostly by fitting the first harmonic normalised second harmonic signal, e.g. 2*f*/1*f*, of the modulated laser transmission. The path-integrated absorbance extracted from the fitting results can be used to calculate the gas properties, e.g. species concentration and temperature, with high sensitivity and fast response [1, 3, 8].

Given the 2*f*/1*f* signal, the spectral-fitting routine is commonly employed to calculate the path-integrated absorbance. In general, the spectral-fitting routine is implemented by least square fitting the 2*f*/1*f* signals from a simulated spectra to an experimental spectra. However, the fitting process can introduce measurement noise caused by the unknown shift of the central wavelength of the laser. In addition, the fitting process inevitably introduces massive and time-consuming repeated iterations until the iteration converges [3, 8]. These limitations, consequently, hinder the application of TDLAS where high-precision and rapid measurement is highly demanded.

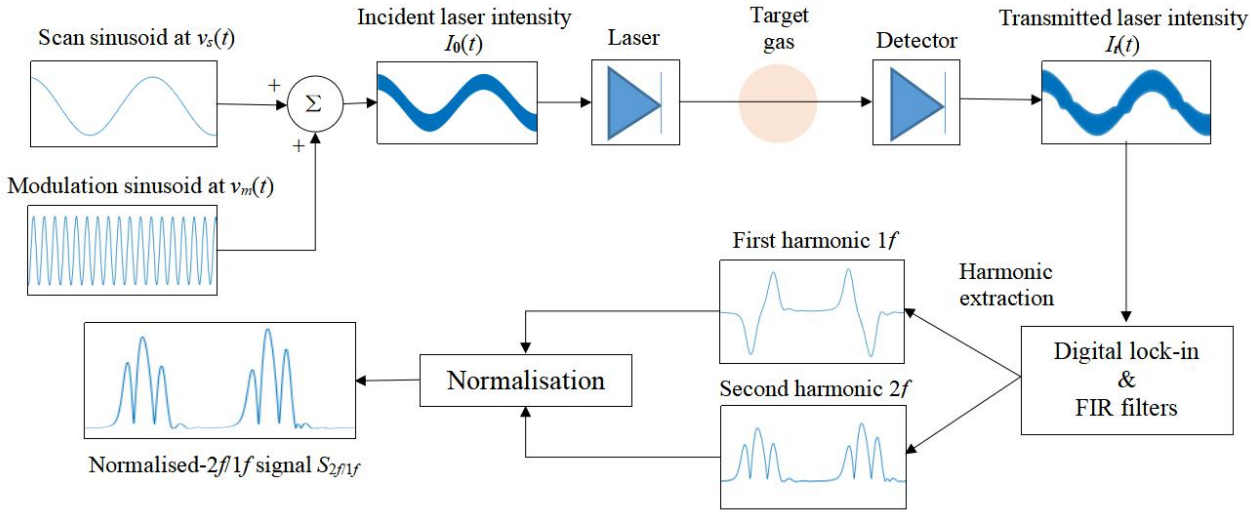

Fig. 1. Schematic of the scanned-WMS and calibration-free processes.

In the past decades, research in the field of machine learning, one of the most crucial topics of artificial intelligence at present, has been rapidly developed, due to the advantages of high efficiency, remarkable stability and automation [10, 11]. In this paper, a noise-resistant approach with a relatively low computation cost is proposed by employing the machine learning regression algorithms. Simulation was carried out to model massive 2*f*/1*f* signals and corresponding path-integrated absorbances taken as training sets and labels. After network training and optimisation, ANN takes the measured 2*f*/1*f* signals as testing inputs, and computes their corresponding path-integrated absorbances at an immensely fast speed. Finally, experiments were carried out to validate the proposed method in terms of noise resistance and computational speed.

II. Methodology

In this section, the detailed WMS technique, traditional spectral-fitting routine and new approach based on machine learning are demonstrated step by step.

A. Fundamentals of WMS

Fig. 1 depicts the flow chart of the typical scanned-WMS absorption system. In general, the laser diode is driven by a high-frequency modulation sinusoid superimposed on a low frequency sinusoid [1-3, 6, 8, 9]. The accurate absorbance can be demodulated from the transmitted light intensity, and has strong resistance to the environmental noise [1, 3, 5, 12]. The modulated wavenumber can be expressed as Eq. (1):

$$v(t) = v_0 + v_s(t) + v_m(t) \tag{1}$$

where v_0 is the central wavenumber according to a specific transition of the target specie, $v_s(t)$ and $v_m(t)$ are the scanning and modulation wavenumbers, respectively. Eq. (2) describes the modulated incident laser intensity $I_0(t)$:

$$I_0(t) = I_c + I_{0,s}(t) + I_{0,m}(t) \tag{2}$$

where I_c is the central average laser intensity, $I_{0,s}(t)$ and $I_{0,m}(t)$ are the scanning and modulation intensity, respectively.

The modulated incident laser intensity $I_0(t)$ passes through the target gas and is detected by photodiode detectors. According to the Beer-Lambert law, Eq. (3) shows the relationship between the incident laser intensity $I_0(t)$ and the transmitted laser intensity $I_t(t)$:

$$I_t(t) = I_0(t) \cdot e^{-\alpha(v(t))} \tag{3}$$

where $\alpha(v(t))$ means the wavenumber-depended absorbance. Provided that the target gas is a homogeneous medium whose temperature and concentration is uniform distributed; the absorbance can be further described as Eqs. (4) and (5):

$$\alpha(v(t)) = -\ln(I_t(t)/I_0(t)) = P \cdot X \cdot S(T) \cdot \phi(v(t)) \cdot L \tag{4}$$

$$A = \int_{-\infty}^{\infty} \alpha(v(t))\ dv = P \cdot X \cdot S(T) \cdot L \tag{5}$$

where P represents the total pressure; L means the length of the laser path; $S(T)$ is temperature-depended line strength; $\phi(v(t))$ is the wavenumber-depended absorption lineshape function; X and T are the uniform concentration and temperature along the laser path, respectively.

Therefore, with the path-integrated absorbance A derived accurately by computations based on the 2*f*/1*f* signal, the compositions and properties of target gas can be easily obtained with high precision and sensitivity [4-6].

B. Traditional Fitting of CF-WMS Strategy

CF-WMS strategy has been developed for the absorption measurement with harsh environments or unknown hardware-related conditions [1, 8, 13]. Essential harmonics extraction employs digital lock-in analysis and finite impulse response (FIR) low pass filters, in which the transmitted laser intensity $I_t(t)$ is multiplied by reference sine and cosine signals at each n*f*-harmonic, respectively, to expand the X_{nf} (cosine) and Y_{nf} (sine) components [1, 3, 7, 8]. Considering both transmitted and non-absorbing laser intensities, the amplitude of first harmonic R_{1f}, the X_{2f} and Y_{2f} components of the second harmonics are required in the normalisation of the 2*f*/1*f* signal to avoid evaluating the background noises unambiguously. The normalisation process is defined as Eqs. (6) and (7):

$$R_{1f} = \sqrt{X_{2f/1f}^2 + Y_{2f/1f}^2} \tag{6}$$

$$S_{2f/1f} = \sqrt{[(\frac{X_{2f}}{R_{1f}})_{real} - (\frac{X_{2f}}{R_{1f}})_{bg}]^2 + [(\frac{Y_{2f}}{R_{1f}})_{real} - (\frac{Y_{2f}}{R_{1f}})_{bg}]^2} \tag{7}$$

where 'real' represents the components of measured transmitted laser intensity; 'bg' means the components of non-absorbing incident laser intensity. By analysing the 2*f*/1*f* signal $S_{2f/1f}$, the path-integrated absorbance A can be derived by applying spectral-fitting routine, to further determine the essential gas compositions and properties [8]. Fig. 2 depicts the flow chart of steps and iteration processes of the tradition fitting strategy.

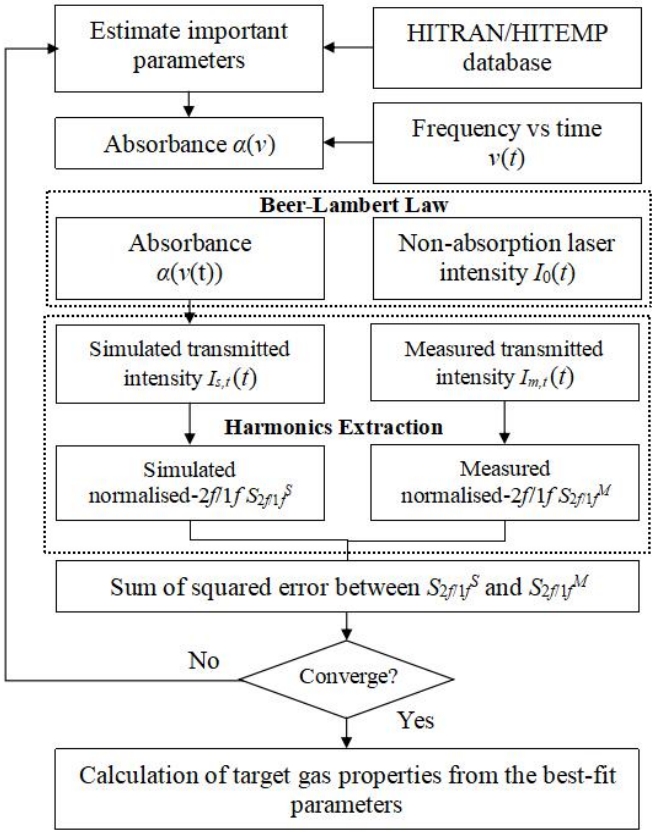

Fig. 2. Flowchart of spectral-fitting method.

Simulation is used to mimic the absorption of target gas on the incident laser intensity passing through it. After the random initialization of required gas properties, the HITRAN database is employed to calculate the absorbances shown in Eq. (4), and the Beer-Lambert law is required to generate the simulated transmitted laser intensity $I_{s,t}(t)$ [1, 3, 4]. The simulated $2f/1f$ signal $S_{2f/1f}{}^{S}$ is obtained after the signal extraction process applying harmonics extraction method and digital lock-in technique. Necessarily, the strategy of least square fitting is repetitively modifications to reduce the sum of squared error between the measured and simulated $2f/1f$ signal $S_{2f/1f}{}^{S}$, which represents the accuracy of currently defined parameters [3]. The traditional fitting strategy displayed in Fig. 2 is mainly based on substantial iterations, calculations and comparisons until the fitting routine converges, indicating the best-fit parameters to determine the gas compositions and properties [1, 3, 13, 14].

C. Enhanced Machine Learning Method

In this approach, a substantial bivariate data set needs to be established firstly, in which N temperature values and N concentration values selected randomly within the maximum demand range are combined as the preparation for simulation. According to Eq. (4), absorbances $\alpha(v(t))$ is proportional to the line strength $S(T)$, and the species concentration X. In the simulation, the combinations of N values of temperature and N values of species concentration results into a data set with length of N^2.

With pure incident laser intensity $I_0(t)$ detected and a set of simulated absorbances $\alpha(v(t))$ obtained, the Beer-Lambert law shown in Eq. (3), can be applied to derive the simulated transmitted laser intensities $I_{s,t}(t)$ of length N^2. Following the same harmonics extraction processes of fitting strategy, the simulated $2f/1f$ signals $S_{2f/1f}{}^{S}$ of length N^2 are processed as training inputs to an initialised ANN, while their corresponding path-integrated absorbances A^S derived previously are defined as regression labels. Generally, each $2f/1f$ signal consists of considerable data points of length M, requiring a high-dimensional machine learning neural network. Therefore, the network structure should conform to the input dimension, which is a $N^2 \cdot M$ matrix. The dimension flow of different stages is depicted in Fig. 3.

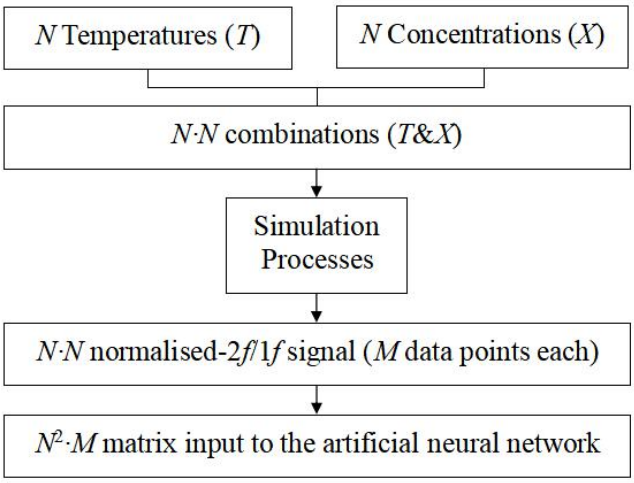

Fig. 3. Data dimensions in different simulation stages.

Main steps and stages are demonstrated as follows:

1) The first step is data pre-processing, where simulation and calculations are carried out based on the temperature and concentration bivariate data set, to obtain the simulated $2f/1f$ signal $S_{2f/1f}{}^{S}$.
2) The simulated $2f/1f$ signals and their corresponding path-integrated absorbances A^S are input as training sets and labels given to the artificial neural network.
3) The shrouded stage is a processing based on the value of each weight and completed in the procedure of weight modification. Applying the backpropagation algorithm based on the gradient descent method, the input training set is processed layer by layer through the hidden networks and transmitted to the output layer repetitively. According to the least square strategy, the sum of squared error between the output of the current neural network and the label is taken as the loss function to justify the conformity and accuracy. If the expected output is not precise and accurate, the backpropagation algorithm will repetitively calculate the partial derivative of each neuron backwards, which is the gradient of each weight and the modification direction, and modify the weight values [10].
4) When the output conforms to its corresponding label's value, the training process proceeds to the optimisation stage. Neural network optimisation, such as adjustments of the length of epochs and batch sizes, determines the absolute accuracy and training period, both of which are essential to be considered.
5) In order to prevent over-fitting, dropout and regularisation are important which could control the magnitude of the parameters to keep the model from becoming too complex and to limit the parameter search space.
6) The ultimate process enters the yield stage. Based on the weights of the concealed units after training, the test sets, consisting of the measured $2f/1f$ signals $S_{2f/1f}{}^{M}$, pass through the completed neural network. The final outputs, predicted path-integrated absorbances A^M, are therefore calculated weight by weight to the output layer.

Following the above procedures, the proposed machine learning approach can accurately compute the predicted integrated absorbances A^M of the measured $2f/1f$ signals, which are defined as testing sets.

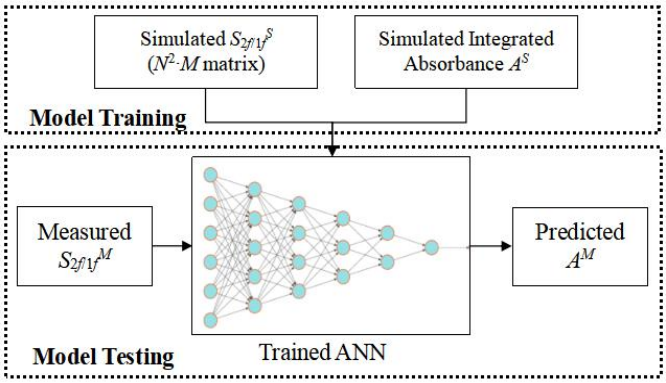

Fig. 4. Flowchart of machine learning processes.

III. Results and Discussion

In this section, the experimental setup, ultimate results after optimisation and comparison with traditional fitting strategy are provided in detail.

A. Experimental setup

Water vapour (H_2O) is selected as the target absorbing species in this work, and we assume that there is no other gases absorbing in this spectral region, which impact the overall absorption. The experiments were carried out using the H_2O absorption transition at 1391.2 nm with ambient pressure and a laser path of 30 cm. The transition is selected due to its relatively high sensitivity within the required temperature range. First, the ranges of temperature T and H_2O concentration X were set 276 K to 1500 K, and 0.01 to 0.15, respectively. As ANN works well for interpolation and very bad for extrapolation, all necessary temperatures and concentrations are taken into account. The ranges take into account all general concentrations and temperatures of not only combustion but non-combustion environments, essentially required in the tomography system. Within the given ranges, 50 evenly spaced points between the maximum and minimum boundaries are generated, resulting in a total of 2500 combinations as the preparation for simulation. Therefore, based on the parameters provided in the HITRAN database and the simulation processes mentioned above, 2500 corresponding sets of simulated $2f/1f$ signal $S_{2f/1f}{}^S$ with their path-integrated absorbances A^S were generated and proceeded to the artificial neural network. The first 2200 sets were selected as the training sets; the other 300 sets were marked as the validation sets, while the path-integrated absorbances A^S act as labels. As single layer neural networks can only be used to represent linearly separable functions, a six-layer artificial neural network was applied, given in Fig. 4, in which the network structure is simplified.

The number of neurons of the four hidden layers depends on the number of input data points and the complexity of the $2f/1f$ signal, the number of input data points in this experiment is 5000, which means the $2f/1f$ signal in both the training sets and the test sets are composed of 5000 points. The first hidden layer consists of 4096 neurons, the second layer consists of 2048 neurons, and the number of subsequent neurons is reduced by a factor of 4. The final number of neurons in the output layer is 1, because there is only one output which is the path-integrated absorbance A. The number of layers and neurons in the artificial neural network was obtained from a large number of experiments to ensure the high stability and accuracy, and to meet the requirements coming from the input data structure and computational complexity. The activation function applied in this experiment and every layer is the 'ReLU' function. Additionally, the dropout and regularisation are used to prevent over-fitting in the training process.

During the training process, the initialisation of the weights can have a significant impact on the results. In this experiment we use a Gaussian distribution initialisation to provide a better initial value for the weights of neurons and to improve the generalisation of the model. After optimisation of the neural network, the well-trained model was employed to receive the testing sets formed by measured $2f/1f$ signals $S_{2f/1f}{}^M$, and predict their corresponding path-integrated absorbances A^M. Therefore, the gas compositions and properties can be obtained according to Eq. (5).

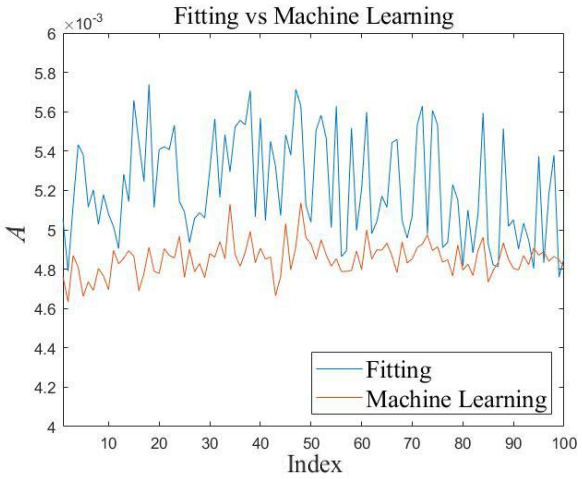

Fig. 5. Results comparison between machine learning and fitting.

B. Experimental results

The measured transmitted laser intensities $I_t(t)$ were repetitively sampled for 100 times in the same environment, from which 100 sets of measured $2f/1f$ signals $S_{2f/1f}{}^M$ were extracted. By feeding the $S_{2f/1f}{}^M$ datasets into the trained regression model, the output, i.e. the path integrated absorbances were obtained. Fig. 5 compares the path integrated absorbances calculated using the traditional spectral fitting routine and the proposed machine learning method.

Obviously, the path-integrated absorbances obtained by machine learning regression algorithms caused much less fluctuation, which means the new data processing introduces lower noise level and carries a higher degree of stability. In terms of statistics, the standard deviation of the fitting strategy results, nearly 2.66×10^{-4}, was approximately three times larger than that of the machine learning approach, which was 8.51 × 10-5.

From the perspective of time cost, the trained machine learning model was able to test massive data sets at an immensely high speed. The above validation model took 0.390625 s to calculate the path-integrated absorbances of 100 sets of 2f/1f signal S2f/1fM, while 0.296875 s was spent on 50 sets of 2f/1f signal S2f/1fM.

However, there is no standard value of the path integrated absorbances in this experiment. The bias differences of fitting method and machine learning can not be calculated to compare the root mean squared error, and therefore the accuracy. Our tasks for the future is to improve the accuracy of the model as much as possible and stabilise the outputs of the neutral network.

IV. Conclusion

This paper demonstrated a new approach for deriving the absorption parameters of target gas using machine learning regression algorithms. Validated by lab-scale experiments of water vapour absorption transition at 1391.2 nm, the

proposed method can half the noise of WMS measurement, in comparison with the traditional spectral-fitting routine. Instead of fitting the harmonics with the time-consuming iterations, the proposed method significantly reduces the computational cost, resulting faster calculation of the path integrated absorbance which computes 100 sets of $2f/1f$ signals in 0.4 s. The machine learning based WMS is potential for rapid spectroscopic computation towards active control of flow fields.

REFERENCES

[1] C. Liu, and L. Xu, "Laser absorption spectroscopy for combustion diagnosis in reactive flows: A review," *Applied Spectroscopy Reviews,* vol. 54, no. 1, pp. 1-44, 2019.

[2] W. V. Drasek, S. Wehe, and M. Allen, "Laser based multiple gas species sensor for harsh combustion process control applications." pp. 1, *Conference on Lasers and Electro-Optics, 2004. (CLEO)*, San Francisco, CA, 2004.

[3] C. S. Goldenstein, C. L. Strand, I. A. Schultz, K. Sun, J. B. Jeffries, and R. K. Hanson, "Fitting of calibration-free scanned-wavelength-modulation spectroscopy spectra for determination of gas properties and absorption lineshapes," *Applied Optics,* vol. 53, no. 3, pp. 356-367, 2014.

[4] R. Arndt, "Analytical Line Shapes for Lorentzian Signals Broadened by Modulation," *Journal of Applied Physics,* vol. 36, no. 8, pp. 2522-2524, 1965.

[5] J. M. Masciotti, J. M. Lasker, and A. H. Hielscher, "Digital Lock-In Detection for Discriminating Multiple Modulation Frequencies With High Accuracy and Computational Efficiency," *IEEE Transactions on Instrumentation and Measurement,* vol. 57, no. 1, pp. 182-189, 2008.

[6] G. B. Rieker, J. B. Jeffries, and R. K. Hanson, "Calibration-free wavelength-modulation spectroscopy for measurements of gas temperature and concentration in harsh environments," *Applied Optics,* vol. 48, no. 29, pp. 5546-5560, 2009.

[7] Z. Qu, and F. M. Schmidt, "In situ H2O and temperature detection close to burning biomass pellets using calibration-free wavelength modulation spectroscopy," *Applied Physics B,* vol. 119, no. 1, pp. 45-53, 2015.

[8] K. Sun, X. Chao, R. Sur, C. S. Goldenstein, J. B. Jeffries, and R. K. Hanson, "Analysis of calibration-free wavelength-scanned wavelength modulation spectroscopy for practical gas sensing using tunable diode lasers," *Measurement Science and Technology,* vol. 24, no. 12, pp. 125203, 2013.

[9] G. B. Rieker, H. Li, X. Liu, J. T. C. Liu, J. B. Jeffries, R. K. Hanson, M. G. Allen, S. D. Wehe, P. A. Mulhall, H. S. Kindle, A. Kakuho, K. R. Sholes, T. Matsuura, and S. Takatani, "Rapid measurements of temperature and H2O concentration in IC engines with a spark plug-mounted diode laser sensor," *Proceedings of the Combustion Institute,* vol. 31, no. 2, pp. 3041-3049, 2007.

[10] S. Shalev-Shwartz, and S. Ben-David, *Understanding Machine Learning: From Theory to Algorithms*, Cambridge: Cambridge University Press, 2014.

[11] F. Azmat, Y. Chen, and N. Stocks, "Analysis of Spectrum Occupancy Using Machine Learning Algorithms," *IEEE Transactions on Vehicular Technology,* vol. 65, no. 9, pp. 6853-6860, 2016.

[12] K. Sun, X. Chao, R. Sur, J. B. Jeffries, and R. K. Hanson, "Wavelength modulation diode laser absorption spectroscopy for high-pressure gas sensing," *Applied Physics B,* vol. 110, no. 4, pp. 497-508, 2013.

[13] D. S. Bomse, A. C. Stanton, and J. A. Silver, "Frequency modulation and wavelength modulation spectroscopies:comparison of experimental methods using a lead-salt diode laser," *Applied Optics,* vol. 31, no. 6, pp. 718-731, 1992.

[14] J. A. Silver, "Frequency-modulation spectroscopy for trace species detection: theory and comparison among experimental methods," *Applied Optics,* vol. 31, no. 6, pp. 707-717, 1992.